Active Segmentation of 3D Axonal Images*

Gautam S. Muralidhar[1], Ajay Gopinath[2], Alan C. Bovik[2], and Adela Ben-Yakar[3]

***Abstract*— We present an active contour framework for segmenting neuronal axons on 3D confocal microscopy data. Our work is motivated by the need to conduct high throughput experiments involving microfluidic devices and femtosecond lasers to study the genetic mechanisms behind nerve regeneration and repair. While most of the applications for active contours have focused on segmenting closed regions in 2D medical and natural images, there haven't been many applications that have focused on segmenting open-ended curvilinear structures in 2D or higher dimensions. The active contour framework we present here ties together a well known 2D active contour model [5] along with the physics of projection imaging geometry to yield a segmented axon in 3D. Qualitative results illustrate the promise of our approach for segmenting neruonal axons on 3D confocal microscopy data.**

I. INTRODUCTION

Understanding the genetic mechanism behind how neurons in the peripheral nervous system repair themselves after injury and how they maintain their axonal structure and function over time holds the key to developing better treatments for neurodegenerative diseases and nerve injuries. This goal has led to recent advances in developing state-of-the art infrastructure using microfluidic devices and femtosecond lasers [1], [2] for performing axotomy on model organisms such as the nematode *C. elegans*. Microfluidic devices enable easy and efficient handling of *C. elegans* for axotomy and imaging without the need for additional immobilizing chemicals, while femtosecond lasers have shown to be valuable as a precise cutting tool for severing axons in *C. elegans* without heating or damaging the surrounding cells. These devices combined with confocal microscopy imaging allow for a study of axonal repair and the associated genetic mechanisms. However, to be able to draw meaningful statistical conclusions, it is necessary to perform high-throughput experiments involving many *C. elegans* worms. High-throughput experiments necessitate automated analysis of the 3D confocal microscopy imaging data after axotomy in order to quantify changes such as re-growth and reconnection that take place along the severed axon. This has resulted in the development of image analysis techniques for quantifying neuronal morphology, e.g., [3] and [4].

In this paper, we present an active contour framework for segmenting neuronal axons, which manifest as open-ended curvilinear structures on 3D confocal microscopy data. Active contour models, also known as *snakes* [6], [7], [8], are commonly employed to represent and track objects of interest in natural and medical images. While the traditional application of active contour models has been the representation of closed regions in images, they have been applied in a few applications involving segmentation of open-ended curvilinear structures [9], [10], particularly in 3D. Finding and modeling open-ended structures such as axons involves unique challenges such as not knowing the length of the axon a *priori*. We address these questions by joining a well known 2D active contour model [5] with projection imaging geometry to yield a 3D segmentation of the axon. Preliminary qualitative results illustrate the promise of our approach for segmenting neuronal axons on 3D confocal microscopy data.

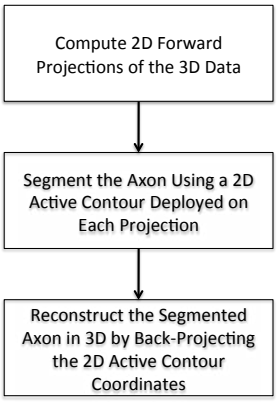

Fig. 1. Proposed framework.

II. PROPOSED FRAMEWORK

The proposed framework is illustrated in Fig. 1. We next describe these steps in detail.

A. Forward Projection

Let $f \in R^N$ represent the vectorized 3D confocal microscopy data, where N is the total number of voxels. Then, for noise-free data, the forward model can be written as:

$$g = Hf, \tag{1}$$

where g is a vector that represents the projection images, and H is the projection matrix, also known as the forward operator. The projection matrix H essentially models the imaging process. For example, the coefficients of H could model the attenuation and linear blur mechanisms inherent in the imaging. The coefficients of H serve as weights that

*This work was supported by the National Institute of Health under grants RO1 NS060129, R21 NS058646, and R21 NS067340.

[1]G. S. Muralidhar is with Biomedical Engineering, The University of Texas at Austin, TX, 78712, USA gautam.sm@utexas.edu

[2]A. Gopinath and A. C. Bovik are with Electrical and Computer Engineering, The University of Texas at Austin, TX, 78712, USA ajay.gopinath@gmail.com, bovik@ece.utexas.edu

[3]A. Ben-Yakar is with Mechanical Engineering, The University of Texas at Austin, TX, 78712, USA ben-yakar@mail.utexas.edu

describe the contribution of each voxel in the data f to a particular projection g_i. We assumed the Radon model while designing the projection matrix H, i.e., only those voxels that lie along a line defined by the coefficients of H contribute to the projection data.

B. 2D Active Contour Model

We next deployed an open-ended parametric 2D active contour on each projection image generated by the forward projection process. A parametric active contour is defined as the parametric curve $v(s) = [x(s), y(s)]^T$, which evolves through the image to minimize the following energy functional [6]:

$$E(v(s)) = \int_0^1 \left[\frac{1}{2}(\alpha|v'(s)|^2 + \beta|v''(s)|^2) + E_{ext}(v(s))\right] ds \quad (2)$$

where $v'(s)$, and $v''(s)$ are first and second derivatives of $v(s)$ that represent continuity and tautness of the curve, respectively. The weighting terms α and β determine how much importance is placed on the continuity and the tautness of the curve, respectively. The terms $v'(s)$, and $v''(s)$ contribute to the internal energy of the contour, i.e., the energy that is inherent in the contour. The term $E_{ext}(v(s))$ determines the external energy typically arising from image features such as edges and is meant to draw the evolving contour towards the boundaries of the object of interest. Typical choices of the external energy include variants of the image gradient [7], [6]. At a local minima of the evolving curve, the Euler-Lagrange force balanced equation $F_{int} + F_{ext} = 0$ is satisfied, where $F_{int} = \alpha v'' - \beta v''''$ is the internal force controlling the curve's continuity and tautness, while $F_{ext} = -\nabla E_{ext}(v)$ is the external force arising from image features such as edges, respectively.

We use the vector field convolution (VFC) formulation for the external energy term [5]. In the VFC formulation, a standard feature map derived from the image is convolved with a user-defined vector field kernel. A requirement on the vector field kernel is that all the vectors in the field should point towards the kernel origin. Hence, when the kernel origin coincides with a feature such as an object boundary or a curvilinear structure, all the vectors in the vector field point towards this feature, causing the evolving contour to be deformed towards the feature. The VFC formulation also provides a large capture range for subtle features of interest and is robust to noise [5].

The feature maps that were convolved with the vector field kernel were derived from the projection images by using a steerable ridge detector that responds to curvilinear structures [11]. The axon seen on each projection image was enhanced on the feature map, as illustrated in Fig. 2. It should be noted that any good off-the-shelf ridge or line detector could be used to derive the feature maps. The only criterion to be satisfied is that the curvilinear structures be enhanced and the background be suppressed.

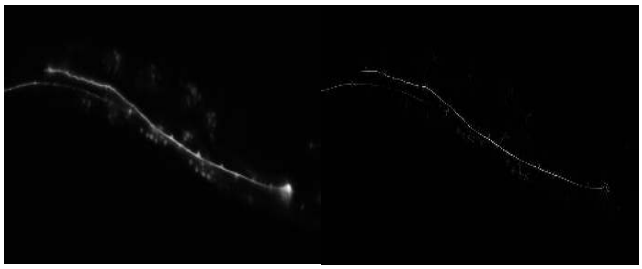

Fig. 2. Left: A projection image depicting the axon. Right: The corresponding feature map depicting the enhanced axon.

C. Active Contour Initialization and Growth

One of the challenges in using a parametric active contour model is the initialization of the curve. We adopt a semi-automatic approach for active contour initialization with a focus on minimal user interaction. Towards this goal, we define the initial curve on each projection image using only two manually marked points on the 3D data that have been projected onto the 2D space. Our approach is driven by the observation that an impulse in a higher dimensional space remains an impulse when projected onto a lower dimensional space. For example, consider the projection of a Dirac singularity centered at (x_0, y_0) in 2D, i.e. the projection of $\delta(x - x_0, y - y_0)$:

$$\begin{aligned} P_\theta(t) &= \int_{-\infty}^{+\infty} \delta(x - x_0, y - y_0)\delta(xcos\theta + ysin\theta - t)dxdy \\ &= \delta(x_0 cos\theta + y_0 sin\theta - t), \end{aligned} \quad (3)$$

where $P_\theta(t)$ is the 1D projection that is the Radon transform of the function $\delta(x - x_0, y - y_0)$. It is immediately evident from (3) that the 1D projection of the 2D impulse is also an impulse, which is located at $t = x_0 cos\theta + y_0 sin\theta$. Using this observation, we manually marked only two end points of each active contour that had to be initialized on the 3D data. These two end points contained in a 3D point volume were then projected onto 2D via the same forward projection process used for the imaging data, as described earlier. The resulting point projections were then automatically processed to retain only the two non-neighboring strongest impulses on each projection image. The initial curve of the active contour was then defined as a straight line segment between these two points on each projection image.

Once the active contour is initialized, the curve deforms iteratively using well known discrete-time coordinate update equations derived from a finite-difference approximation of the Euler Lagrange equation [5]. However, a problem encountered when segmenting open-ended curvilinear structures such as axons, is that the length of the structure is not known a *priori*. To solve this problem, we adopt a scheme that we have used previously to segment open-ended curvilinear structures on mammograms [9]. Essentially, we let the active contour curve alternately grow and deform. To begin with, the curve is defined as a straight line segment between the two point projections. The curve then deforms

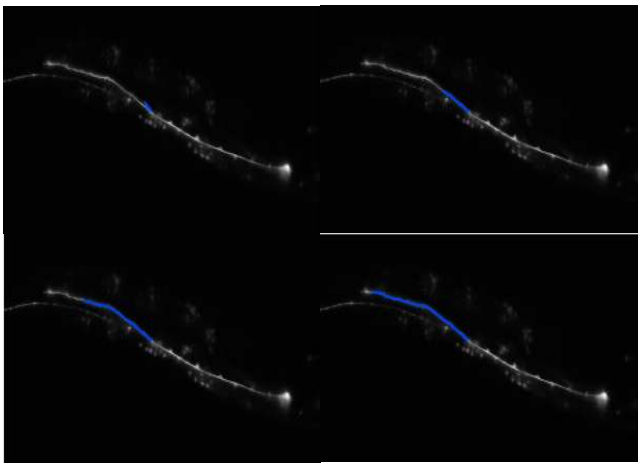

Fig. 3. Growing active contour. top left: initial curve; top right: after 5 iterations; bottom left: after 15 iterations, bottom right: after 25 iterations.

under the influence of its internal and external forces for a fixed number of iterations. The deformation is followed by extending the curve along one of it's end points in the direction of the tangent computed at that end point by introducing another short line segment of a predefined length. This new segment then deforms under the influence of its internal and external forces for a fixed number of iterations. The process of extension and deformation repeats until a stopping criterion is met or a certain number of iterations have been completed. We do not use a stopping criterion but rely on a fixed number of iterations, though a stopping criterion based on factors such as curvature could easily be incorporated. For instance, in our previous work [9], we have used a curvature based stopping criterion for open-ended active contours, where the growth of the contour was terminated at a point where the curvature exceed a 30° limit. The predefined length of each extended straight line segment was set to an arbitrarily chosen value of 10 pixels and the number of iterations of extension and deformation was set to 25. Fig. 3 illustrates four iterations of the growing active contour along an axon trajectory on one of the projection images.

D. 3D Reconstruction of the Axon

Once the 2D active contours have been deployed on each projection image and the axon has been segmented in 2D, reconstruction of the 3D axon is performed using the simple back-projection operator H^T, i.e.

$$f_{seg} = H^T g_{seg}, \tag{4}$$

where g_{seg} is the vectorized projection data containing non-zero values only along the active contour coordinates. The result of this operation yields the segmented axon in 3D.

III. EXPERIMENTS AND RESULTS

The data set for this study comprised of a stack of 51 confocal microscopy images depicting the anterior longitudinal microtubule (ALM) - a touch receptor neuron in the *C. elegans* worm. The theoretical resolution of the data was 149 nano-meters in the x-y plane, while the resolution along the optical axis of the microscope (z-direction) was 529 nano-meters. Each image was 2048×2048 pixels in dimension with 8 bits per pixel. Hence, the dimensions of the 3D volume was $2048 \times 2048 \times 51$ voxels. For efficient processing, we considered a cropped 3D volume that best depicted the axon. The dimensions of the cropped volume was $1549 \times 901 \times 28$ voxels. The forward projections were then computed on the cropped volume. For the forward projection Radon model, we considered 91 angular increments from -45 to + 45 degrees. Each projection image was further sub-sampled by a factor of two to accelerate processing. The active contours and the subsequent 3D reconstruction of the segmented axon were then carried out on the sub-sampled projections. We manually initialized two pairs of end points on a 3D slice best depicting the region where the axon had been severed. These two pairs of points were then projected onto the projection space using the same forward projection model used for the imaging data. The projected points are illustrated in Fig. 4 along with the region where the axon was severed. Also illustrated in Fig. 4 are the original and axon re-growth trajectories pre- and post-axotomy. The 3D rendering of the segmented axon trajectories is illustrated in Fig. 5. We used the open source software VolRover (`http://cvcweb.ices.utexas.edu/cvcwp/?page_id=100`) to perform 3D volume rendering and visualization. It is evident from Fig. 5 that the two active contours were able to capture, segment, and accurately represent the original axon trajectory as well as the re-growth trajectory after axotomy.

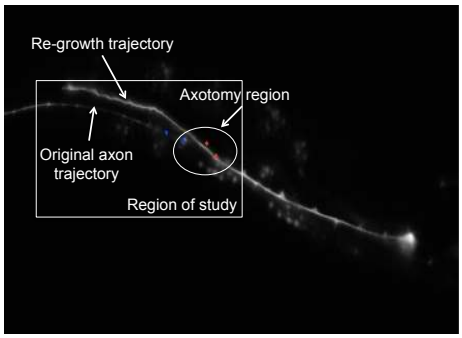

Fig. 4. Two pairs of initial active contour end-points on a projection image. The blue points represent one pair, while the red points represent the other. Also illustrated are the axotomy region and the two trajectories of the axon pre-and post-axotomy.

IV. CONCLUSION

We have presented a framework for reconstructing and representing neuronal axons in 3D from confocal microscopy imaging data. The basic framework can be extended to represent open-ended curvilinear structures on other multi-slice imaging modalities that follow the principles of projection imaging geometry. Future work includes a quantitative validation of the framework, and modeling the repair and regeneration of multiple 3D neuronal axons from confocal microscopy images acquired after axotomy on a large number of *C. elegans* worms.

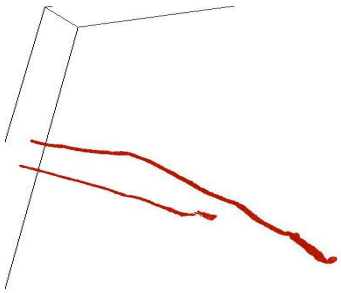

Fig. 5. 3D rendering and visualization of the active contours.

ACKNOWLEDGMENT

The authors would like to thank Frederic Bourgeois for acquiring and supplying the confocal microscopy data.

REFERENCES

[1] S. X., Guo, F. Bourgeois, T. Chokshi, N.J. Durr, M. Hilliard, N. Chronis, and A. Ben-Yakar, Femtosecond laser nanoaxotomy lab-on-a-chip for in-vivo nerve regeneration studies, *Nature Methods*, vol. 5, pp. 531-533, Jun. 2008.

[2] F. Yanik, H. Cinar, N. Cinar, A. Chisholm, Y. Jin, and A. Ben-Yakar, Neurosurgery: Functional regeneration after laser axotomy, *Nature*, vol. 432, pp. 822, Dec. 2004.

[3] Y. Zhang, X. Zhou, J. Lu, J. Lichtman, D. Adjeroh, and S. T. C. Wong, 3D axon structure extraction and analysis in confocal fluorescence microscopy images, *Neural Computation*, vol. 20, pp. 1899-1927, Aug. 2008.

[4] D. E. Donohue and G. A. Ascoli, Automated reconstruction of neuronal morphology: An overview , *Brain Research Reviews*, vol. 67, pp. 94-102, Jun. 2011.

[5] B. Li and S. T. Acton, Active contour external force using vector field convolution for image segmentation, *IEEE Transactions on Image Processing*, vol. 16, pp. 2096-2106, Aug. 2007.

[6] M. Kass, A. Witkin, and D. Terzopoulos, Snakes: active contour models, *International Journal of Computer Vision*, vol. 1, pp. 321-331, Apr. 1988.

[7] X. Chenyang and J. L. Prince, Snakes, shapes, and gradient vector flow, *IEEE Transactions on Image Processing*, vol. 7, pp. 359-369, Mar. 1998.

[8] T. F. Chan and L. A. Vese, Active contours without edges, *IEEE Transactions on Image Processing*, vol. 10, pp. 266-277, Feb. 2001.

[9] G. S. Muralidhar, A. C. Bovik, J. D. Giese, et al., Snakules: A model-based active contour algorithm for the annotation of spicules on mammography, *IEEE Transactions on Medical Imaging*, vol. 29, pp. 1768-1780, Oct. 2010.

[10] M. B. Smith, L. Hongsheng, T. Shen, et al., Segmentation and tracking of cytoskeletal filaments using open active contours, *Cytoskeleton*, vol. 67, pp. 693-705, Nov. 2010.

[11] M. Jacob and M. Unser, Design of steerable filters for feature detection using Canny-like criteria, *IEEE Transactions on Pattern Analysis and Machine Intelligence*, vol. 26, pp. 1007-1019, Aug. 2004.